Indian Journal of Pure & Applied Physics
Vol. 62, February 2024, pp. 77-86
DOI: 10.56042/ijpap.v62i2.7709

Tuning of the Plasmonic Response Gold and Aluminum Nanoarrays for Sensing Applications

Gaurav Pal Singh[a], Raj Harsh[b] & Neha Sardana[a*]

[a]Department of Metallurgical and Materials Engineering, Indian Institute of Technology Ropar, Rupnagar 140 001, India

[b]Department of Materials and Metallurgical Engineering, Punjab Engineering College (Deemed to be University), Chandigarh 160 012, India

Received: 1 January 2024; accepted: 23 January 2024

Nanoarrays are at the forefront of research and commercial plasmonic devices. The shape, size, periodicity and material of the structures in nanoarrays determine their optical response. Therefore, the performance and operating wavelength range of the nanoarrays can be tuned by the aforementioned parameters. Disc, square and triangular nanoarrays of gold and aluminum were compared using finite element method (FEM) simulations. The effect of size, thickness and periodicity was studied in detail. The coupling effect of the resonant modes observed in the nanoarrays resulted in a sharp resonance in the transmission spectra, which could be used for next generation chemical and biosensors. Gold nanoarrays had stronger resonance in the visible spectrum. Aluminum nanoarrays displayed resonant modes in the UV region, which were absent for gold. However, weak resonances for aluminum were seen in the visible region due to the increased losses. Sensitivity of nanoarrays was compared to quantify their performance. The coupling of the lattice resonance with the single structure resonance had a major impact on the sensing performance. Nanoarray with gold triangles at the optimal coupling condition (wavelength of lattice resonance equal to the single triangle) showed the highest sensitivity, 541 nm/RIU, which was also compared to the sensing substrates in literature. Shapes with more potential for hotspots were considered highly suitable for sensing applications.

Keywords: Plasmons; Localized surface plasmon resonance (LSPR); Sensing; Gold nanoparticles

1 Introduction

Humans have been inspired by nature to employ the power of structured surfaces to manipulate light for various applications. A butterfly's wings are one such example in nature that uses periodic structures on surfaces to create complex patterns and bright colours due to the dimensions of the structures[1]. Periodic structures when reduced to sizes close to or less than the wavelength of incident light, lead to a unique response based on the geometry and morphology of the structures[2]. Therefore, to capitalize on the structures' response in the visible wavelength range, their size has to be in a few hundreds of nanometres. Furthermore, nano structures fabricated using materials showing good plasmonic response such as Au, Ag, Al, Cu, *etc*. have been on the forefront of cutting-edge technologies. Some of the applications of plasmonic structured surfaces in the visible regime are sensing[3], antireflective coatings[4], highly absorptive solar cells[5], high speed optoelectronic devices [6], *etc*.

A plasmon refers to the collective excitation of electrons in response to an electromagnetic (EM) wave[7]. In practical applications, this collective excitation is generally obtained as localized surface plasmon resonance (LSPR) and surface plasmon resonance (SPR). Metals show a good plasmonic response due to the availability of free electrons on their surface[8]. The LSPR condition is satisfied in structures that are comparable to or smaller than the wavelength of the incoming EM wave. The electrons on the surface of these structures collectively oscillate to oppose the incoming EM wave, further, at the resonance condition, the oscillation frequency matches with the incident EM wave[9]. SPR is observed in metallic films with thickness in tens of nanometres, however, SPR condition is not fulfilled directly by a thin metal film. The momentum of the incoming EM wave must match the momentum of the surface plasmons. The simplest method of satisfying the SPR condition is by using the Kretschmann configuration, which uses a prim that creates an evanescent wave via total internal reflection to satisfy the coupling condition[10]. Another method to obtain the momentum matching is by creating a grating like structure on the thin film, which is called grating coupling/resonance[11]. The plasmons in the case of

*Corresponding author: (E-mail: nsardana@iitrpr.ac.in)

thin films are no longer confined as in LSPR, but propagate as surface plasmon polaritons (SPPs). At the resonance condition, the frequency of the frequency of SPPs is equal to the incoming EM wave.

The dielectric function of a material determines the intensity and wavelength range of its plasmonic response[12]. Ag and Au have the best plasmonic response among the commonly available materials; however, Ag is highly prone to corrosion [13]. Hence, Au is highly prevalent as a plasmonic material throughout research and commercial applications. The research community is on the hunt for new economic materials which can replace Au, the best candidates are Cu and Al. Comparison of the dielectric function and LSPR response of Ag, Au, Al and Cu shows that, the wavelength of the plasmonic response of Ag, Au, and Cu was similar and in the visible range. However, the intensity of response was the highest for Ag, followed by Au and then Cu, owing to the imaginary part of the dielectric function in the visible range. A larger imaginary part of the dielectric function leads to more losses in the material, thereby causing a lower intensity of the plasmonic response. Al in comparison, showed plasmonic behaviour in the UV and visible wavelength, but it also had high losses similar to Cu[14].

Apart from the material effect; the size, shape, and periodicity of the structure have a critical impact on its overall plasmonic response. The fabrication methods employed by engineers and scientists to fabricate nanostructures include electron beam lithography (EBL)[15], UV lithography[16], laser interference lithography[17], nano imprint lithography[18], and templating methods which use nanospheres [19]and anodic aluminium oxide (AAO) arrays[20]. Nishijima *et al*.[21] presented the effect of periodicity on the plasmonic resonance of gold nanodisk arrays for applications in light harvesting and solar cells. EBL was used to fabricate the arrays on a glass substrate. EBL is the method with the highest resolution and is able to create periodic as well as non-periodic structures; however, the technique is slow and very expensive[22]. The remaining techniques use templates to create periodic structures, which can then be selectively deposited with the required material and thickness, and the excess material is etched away. Thereby, these techniques can create arrays of nanosized shapes of plasmonic materials on the required substrate. The highly prevalent shapes for plasmonic applications include nanoarrays of disc, square and triangle shaped structures in a square lattice. Potejanasak[23] used an economical nano imprint method to fabricate a nanodisk array on a glass substrate for sensing applications. The method was deemed suitable for mass production. Further, altering the shape of the shapes in the nanoarrays leads to higher confinement of the EM wave by the creation of hotspots. Luo *et al*. [24] used nanosphere lithography for high throughput fabrication of arrays containing gold triangles on a glass substrate. The triangular nanoarray was used as a surface-enhanced Raman spectroscopy (SERS) substrate which showed huge enhancement of the Raman signal and was able to detect dye molecules at the pico Molar concentrations. Mudachathi and Tanaka[25] created a tuneable square Al array to replicate the dazzling colors seen in butterflies and peacocks. It was observed that the colors seen in the square nanoarray could be altered by varying the size of the square and the periodicity of the array. As previously explained, the LSPR and SPR conditions have different excitation conditions. The nanoarrays displayed a combined effect of LSPR (due to the size of the individual shape being comparable to the incoming EM wave) and grating resonance. Therefore, nanoarrays have the potential to reap the benefits of both lattice and single structure resonance modes. Furthermore, the interference of the various resonance modes in metal and/or dielectric structures arranged in a periodic lattice can create exciting properties such as electromagnetically induced transparency (EIT)[26]. This phenomenon was generally observed at the quantum level for many years, however, recently nanoarrays have shown to create destructive interference of normal modes that create windows for very high Q factors and figure of merits (FOM). The main resonant modes include single structure resonance (which is also referred to as LSPR and Mie localized resonance) of one or more than one structures and lattice resonance (which is also referred to as grating resonance). Also, the single structure can support dipole, quadrupole, and other higher order poles. There are 2 major methods using which a very high Q factor windows can be created, interference of two or more single structure resonance modes (bright and dark modes)[26] and interference of single structure and lattice resonance mode. This destructive interference leads to a drastic decrease in group velocity of light which has opened up the potential numerous new technologies. The

applications of EIT are in optical communications and computation (increasing the speed and decreasing power compared to electronic switches), light delay and storage[27], enhanced non linear optics[28], biomedical imagining and new age sensing substrates. Another interesting property observed in nanoarrays is electromagnetically induced absorption (EIA)[29], as opposed to EIT, constructive inference enhances the absorption of light in a specific wavelength range. The applications include non linear spectroscopy, lasers and optical amplifiers.

The current article aims to improve the understanding of the resonant modes in a nanoarray placed in a non-homogenous medium (air-glass interface) for sensing applications. Single structure resonance, grating resonance, as well as their coupling effect is presented. First, the effect of geometric parameters (diameter, thickness and periodicity) of gold nanodisk arrays of Au and Al are compared. Then, the disc shape is compared with square and triangle, to observe the effect of increased hotspot generation on their overall plasmonic response and sensitivity. Although discussion of nanoarrays is prevalent in literature, the discussion covering material effect, the single structure response, lattice and structure resonance coupling, and sensitivity analysis is lacking.

2 Material and Methods

In the field of space and time dependent problems within the domain of physics, the governing laws are often described through partial differential equations (PDEs). Unfortunately, the analytical solutions for these PDEs are elusive for the majority of geometries and scenarios. As a pragmatic alternative, approximations of these equations are formulated, typically employing various discretization techniques. These methods involve representing the continuous PDEs as numerical model equations, which can then be tackled using numerical methods. The finite element method (FEM) stands out as a prominent approach for generating such approximations. By utilizing FEM, one can discretize the problem domain into finite elements, allowing for the creation of a system of algebraic equations. Solving these equations provides a numerical solution to the model, serving as an approximation to the actual solution of the original PDEs. This indispensable methodology plays a crucial role in tackling complex physical problems that resist analytical resolution, offering a practical means to obtain valuable insights into the behavior of dynamic systems. Overall, the FEM stands out for its flexibility in discretization, allowing users to freely choose elements for spatial discretization and basis functions. FEM is widely used in literature for obtaining accurate solutions for plasmonic structures[30].

The simulation study was performed on commercial software COMSOL Multiphysics, which uses FEM to solve Maxwells equations. The following wave equation is considered in the simulation domain:

$$\nabla \times \left(\frac{1}{\mu_r}\nabla \times E\right) - k_0^2 \varepsilon_r E = 0 \quad \ldots (1)$$

where, ε_r and μ_r are the relative permittivity and permeability, respectively. k_0 represents the incident wave vector and E is the electric filed vector[31]. The above equation allows the calculation of the far field optical response. To quantify the near field electric field, the EM wave perpendicular to the nanoarray with the wave vector k_0 is oriented parallel to the z axis. The electric field E corresponds to linearly polarized light. The computation is performed in the wavelength domain, allowing the removal of the oscillation factor $e^{i\omega t}$ from E as:

$$E = \hat{E}|E_0|e^{i\omega t} \quad \ldots (2)$$

where, the amplitude of the electric field is denoted by the absolute value of E_0. $\hat{E}$ is the unit vector pointing at the direction of polarization. The dielectric function of Aluminum [32]and Gold [32]was input in the form of Drude-Lorentz model, which can be described as:

$$\varepsilon(\omega) = \varepsilon_\infty - \omega_p^2/(\omega^2 - i\omega\omega_\tau) \quad \ldots (3)$$

where, ε_∞ signifies the influence of bound electrons on the relative dielectric constant, while ω_p denotes the plasma frequency and ω_τ represents the damping frequency.

The 3D simulation domain consisted of a nanoarray placed at the interface of materials with refractive index n_1 and n_2 as show in Fig. 1(a). To induce the array effect, the floquet periodic condition was applied at the opposing faces[33]. The EM wave traveled from the top to the bottom of the simulation domain via two ports. The upper and lower boundaries of the simulated array domain were also equipped with perfect matching layer (PML) boundary conditions to absorb the unwanted scattered fields[34]. Glass was considered the substrate, thereby, the refractive index n_2 was 1.5. The simulation was performed for nanopatterns with disc, triangular, and

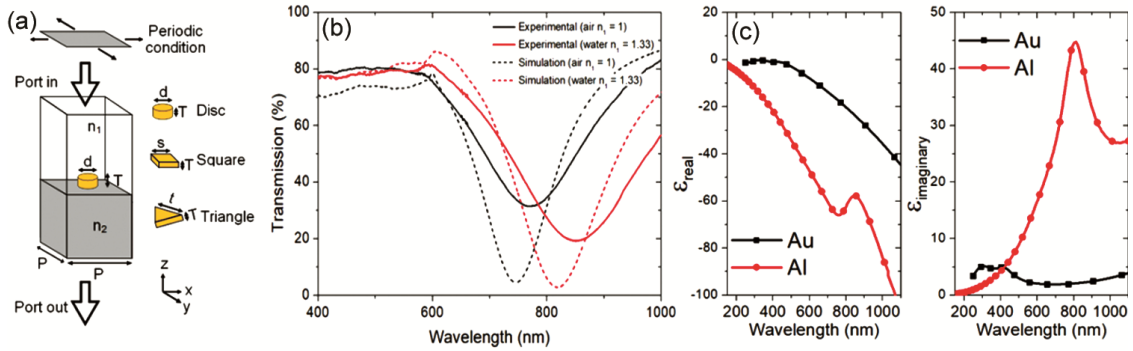

Fig. 1 — (a) Simulation domain showing the ports, periodicity and the shapes that were analyzed. The periodicity (P), thickness (T), diameter (d), and sides (s and t) were varied. (b) Comparison of simulation and experimental results of 400 nm period, 187 nm diameter and 45 nm thickness. (c) Real and imaginary part of the dielectric function of Au and Al according to Lorentz Drude model.

squares. To compare the three shapes, the volume of the shapes was kept the same. Fig. 1(a) shows the various shapes and the geometric parameters studied in the current article. To calculate the transmission spectra of the various nanoarrays, the simulation was performed from wavelength 200 nm to 1800 nm. Initially, the effect of thickness (10 nm to 150 nm) with period to diameter ratio of 0.5 for Au and Al nanodisks of diameter 50 nm, 100 nm, 200 nm, and 300 nm was seen. Then, the effect of periodicity (diameter to periodicity ratio 0.2 to 0.8) for the aforementioned nanodisks with thickness 30 nm was calculated. The coupling effect was most clearly observed in 200 nm nanodisks (explained in results and discussion section); hence, it was selected for further analysis. Similar thickness and periodicity studies were performed for square and triangle shapes with volume equal to disc of diameter 200 nm and thickness 30 nm. Sensitivity analysis was performed for the optimal coupling periodicity.

The simulation was validated using experimental results; the comparison is shown in Fig. 1(b). The nanodisks were fabricated using laser interference lithography (LIL). Briefly, photoresist was spin coated on a glass substrate. Lloyd's mirror setup was used to double expose (90° rotation of the second exposure) the photoresist to a deep UV laser (266 nm and 30 mW) for 110 seconds (for each exposure). The angle of incidence of the laser beam was selected such that the periodicity of the array was 400 nm. The sample was developed and 5 nm chromium and 40 nm of gold was deposited using a thermal evaporator. The transmission spectra were measured using a StellarNet spectrometer in air (n = 1) and water (n = 1.33) surrounding the nanodisk array (on the glass substrate) as shown in Fig. 1(b). The discrepancy in the resonance wavelength was less than 4 % a stronger resonance was observed compared to the experimental spectrum. It was deemed to be due to the practical losses and imperfections in the experimental nanoarray.

3 Results and Discussion

3.1 Effect of geometric parameters (thickness, diameter, and periodicity)

The selection of geometric parameters is a critical aspect for any plasmonic application. Generally, the disc nanoarray is the easiest to fabricate by the methods listed in the introduction section. Furthermore, in many of the techniques, the period to diameter ratio (d/P) is usually around 0.5. Therefore, the Au disknanoarray on a glass air interface of diameters 50 nm, 100 nm, 200 nm, and 300 nm are compared with d/P 0.5 in the Fig. 2(a-d). A strong resonance in the transmission spectra was observed in Fig. 2(a, b). In the near field, the creation of a dipole was observed in the electric field contour, as shown in Fig. 5 (d). Increasing the thickness leads to a blue shift in the transmission dip, this is due to an increase in the surface charge of the nano sized disc[35]. The increase in size diameter causes a red shift of the transmission dip. The larger size creates a lower surface charge density, which leads to a weaker restoring force of the oscillating dipole and hence, a decreased resonance frequency[36,37]. Further, the increase in size also increases the size of the localized plasmon,whichis comparable to the size of nanodisk[38]. Therefore, the increased size also causes higher radiation damping that increases the full width at half maxima (FWHM) of the dipole resonance[38]. Now, for the 200 nm diameter disc, a Fano like resonance can be clearly observed at 600 nm for all the thicknesses that are plotted in the Fig. 2 (c). This Fano resonance is due to a

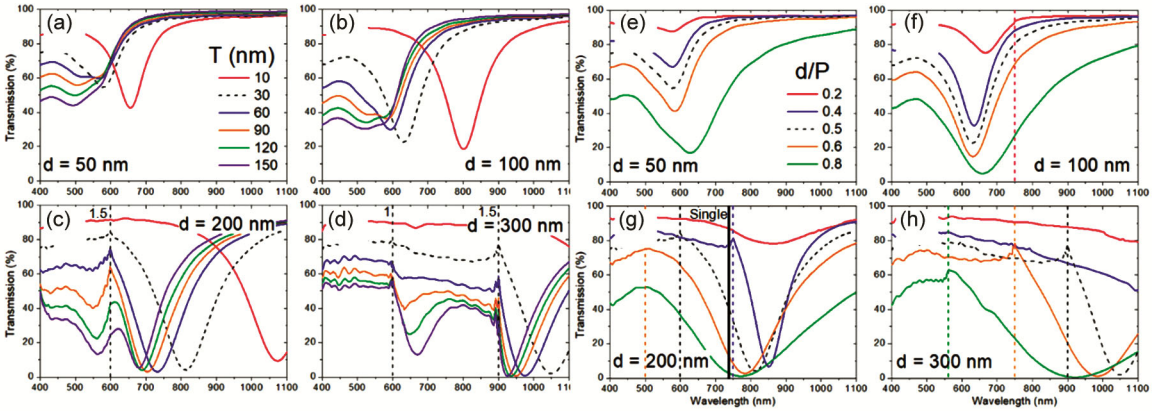

Fig. 2 — Simulated transmission spectra for Au disc nanoarray at air glass interface. (a-d) Thickness variation and (e-f) variation of d/P. The vertical dashed lines represent lattice resonance,(1 0) diffraction edge,and the number beside is the refractive index for the lattice resonance. No number pertains to the resonance due to glass environment (n=1.5). Solid line represents the single disc resonance.

lattice effect in the surrounding refractive index, which can be approximated using the following general equation[39].

$$\lambda = n P \quad \ldots (4)$$

where λ represents the resonance wavelength, n is the refractive index of the surrounding. The 600 nm lattice resonance is due to the 1.5 refractive index of the glass substrate. Increasing the thickness creates a higher conferment of the EM wave; therefore, for larger thicknesses, along with a dipole at larger wavelengths, an octupole resonance[40] can be observed at the shorter wavelengths as shown in Fig. 5(d). Moving to an even greater diameter of 200 nm, along with the lattice resonance due to glass surrounding at 900 nm, another lattice resonance can be observed at 400 nm due to the refractive index of air (n =1).

The effect of periodicity is observed by varying the d/P ratio for the various diameters of the disc nanoarray as shown in Fig. 2 (e -h). It was observed that at smaller d/P (for very large periodicity), the resoaonce intensity was very low, and it increased as d/P was increased (the periodicity becomes closer to the diameter of the disc). For larger d/P, the higher confinement of the EM wave creates a strong plasmonic response. The dashed lines represent the lattice resonance for the respective colored d/P. An interesting observation can be made for 200 nm diameter disc nanoarray (Fig. 2(g)). The major transmission dip had a very strong resonance for the d/P ratio of 0.4. It was noted that the single particle resonance for 200 nm diameter Au disc is at 895 nm, represented by the solid black line. It was observed that the strongest resonance (had the lowest transmission dip) for the d/P ratio for which the lattice resonance was the closest to the single particle resonance. As the lattice resonance moved further away from the single particle resonance, the intensity of the major resonance decreased. Hence, it can be concluded that the coupling of the single particle and lattice resonance creates a highly intense transmission dip[41]. For a 300 nm diameter disc nanoarray, the single particle resonance was at 1152 nm (far away from the lattice resonance), and the lattice resonance dominates the single particle resonance. Meanwhile, for 50 nm and 100 nm diameter, the single particle resonance (at 592 nm and 664 nm, respectively) dominates the transmission spectra. Therefore, to observe the coupling effect in other shapes (square and triangular nanoarrays), where the volume is kept equal to the diameter 200 nm disc. The comparison of the various shapes is presented after the discussion of Al disc nanoarray.

3.2 Effect of change of material

To study the effect of the change in material to the response of the nanopattern array, the extinction cross section spectrum of single nanostructures of volume equivalent to disc of diameter 200 nm and thickness 30 nm (shown in Fig. 3). Considering a nanodisk of Au and Al, it was clearly observed that a strong dipole resonance was seen for both. However, for Al, the resonance was blue shifted, had a higher FWHM, and was of lower intensity. To explain this change in the response of the nanodisk, the dielectric function of Au and Al, shown in Fig. 1(c) will be used. The blue shift was due to the large negative real part of the dielectric function achieved for shorter wavelength in Al as compared to Au. The broader and less intense

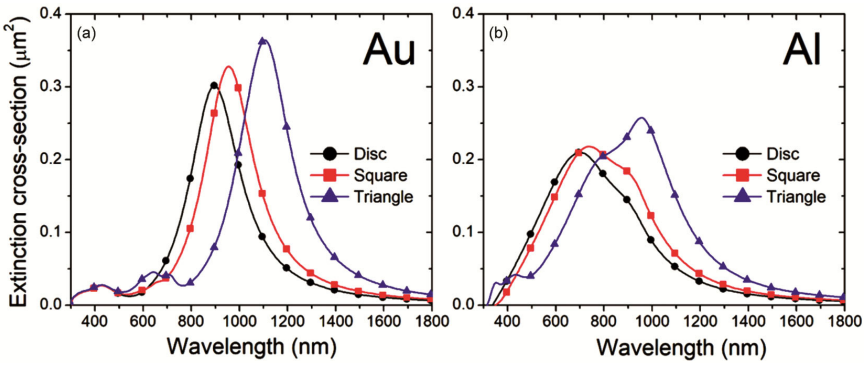

Fig. 3 — Extinction cross section of single nanostructures (disc, square, and triangle) with volume equivalent to a nanodisk of diameter 200 nm and thickness 30 nm of a) Au and b) Al (polarization direction is same as for Fig. 5).

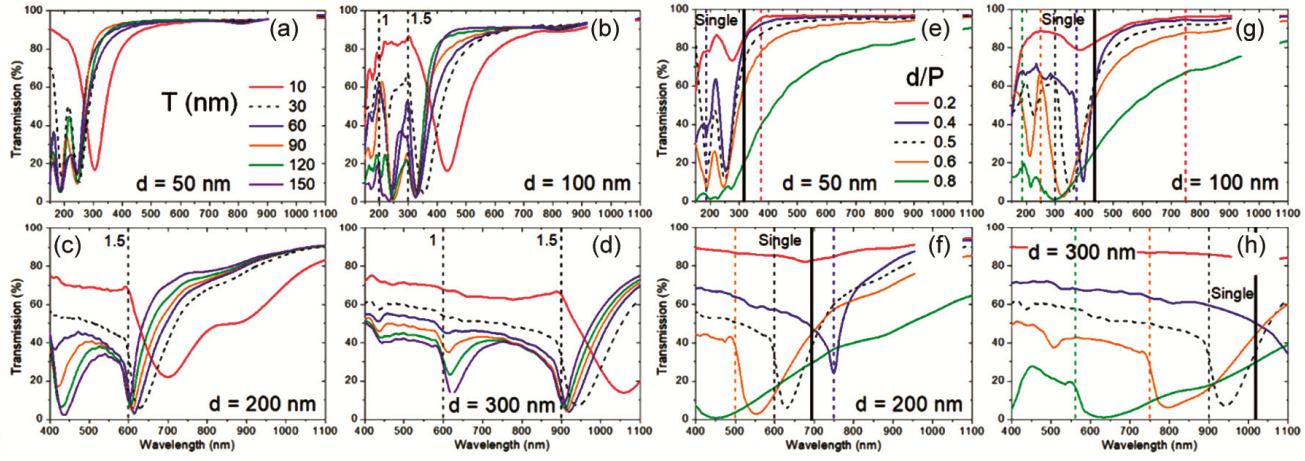

Fig. 4 — Simulated transmission spectra for Al disc nanoarray at air glass interface. (a-d) thickness variation and (e-f) variation of d/P. The vertical dashed lines represent lattice resonance, (1 0) diffraction edge, and the number beside is the refractive index for the lattice resonance. No number pertains to the resonance due to glass environment (n=1.5). Solid line represents the single disc resonance.

resonance was due to the large positive imaginary part of the dielectric function.

Now, when the nanodisks were arranged in a square lattice, it was observed that the dipole resonance of Al for similar sizes was blue shifted, and a strong resonance in the transmission spectra was also observed in the UV region as shown in Fig. 4(a-h). This can be easily observed for 50 nm and 100 nm diameter disc nano array in Fig. 4 (a, b). The distinguishable resonances in the UV region in Al can be explained due to the lower imaginary part of the dielectric function in the UV region (shown in Fig. 1 (c)). However, at larger wavelengths, the transmission dip is broader and less intense in Al because of the increased losses, as compared to Au. The Fano resonance due to lattice effect was seen for diameter 100 nm disc nanoarray also. The other observations for Al disc nanoarray were similar to that of Au nanoarray. For the diameter 200 nm Al disc nanoarray, the single particle resonance for Al was at 691 nm. The highest coupling effect was observed for the d/P of 0.4, for which the lattice resonance was at 750 nm. The red shifted lattice resonance (for d/P 0.5 and d/P 0.6) led to a weaker resonance (higher FWHM), and for the red shifted resonance (d/P = 0.2), the resonance almost disappeared. Also, due to the low losses in the UV region, a big coupling effect was also observed for d/P ratio of 0.4 for diameter 100 nm disc nanoarray (which was absent for Au nanodisk array).Therefore, the material and the geometric parameters play a critical role in determining the plasmonic response of the nanoarray.

3.3 Effect of change of shape

To analyze the effect of the shape of the particle in the nanoarray, square and equilateral triangle shapes were simulated. The sides s (for square) and t (for triangle) were kept at 177.25 nm and 269.35 nm to keep the volume equal to the disc with a diameter

of 200 nm. The size was chosen in order to observe the coupling effect clearly in the selected shapes. The polarization direction for the simulated plots can be seen in Fig. 5 (θ was 0° for the plots in the current article). The extinction cross section plots in the Fig. 3 present the effect of the change in optical response for disc, square and triangle of volume equal to nanodisk of diameter 200 nm and thickness 30 nm. A red shifted and increased dipole intensity in the extinction cross section spectrum can be observed as the shape of the nanostructure was changed from disc to square to triangle. The red shift was majorly due to the increase in size of the structure (both square and triangle) in the polarization direction (the direction is same as for Fig. 5) when the volume was kept equal to the disc. The increase in intensity was due to the creation of electric field hotspots near the sharp corners in square and triangle[14]. The asymmetry in the dipole resonance in Al structures was because of the increased effect of higher order poles.

Simulations were performed for both Au and Al nanoarrays to observe the effect of thickness and periodicity, as shown in Fig. 6 (a-h). The plots displayed a similar trend to that discussed for disc nanoarray. It was observed that for comparable sizes, the major resonances were red shifted due to single particle resonance being at longer wavelengths for both square and triangle. Furthermore, the increased confinement of the EM wave due to the hotspot generation was confirmed by the increased intensity of the resonances. Similar to the disc nanoarray, higher order poles were observed for larger

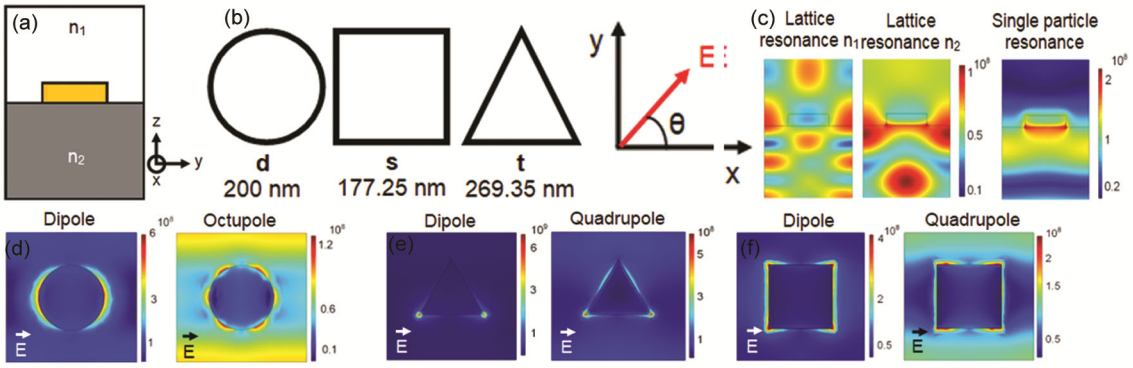

Fig. 5 — (a) Simulation domain of nanodisk array. (b) Various shapes analyzed and the direction of polarization. (c-e) Normalized electric filed in (V/m) contours for the nanoarrays showing (c) lattice and single particle resonances, (d) Dipole and Octupole in disc nanoarray, (e) Dipole and Quadrupole in triangle nanoarray, and Dipole and Quadrupole in square nanoarray.

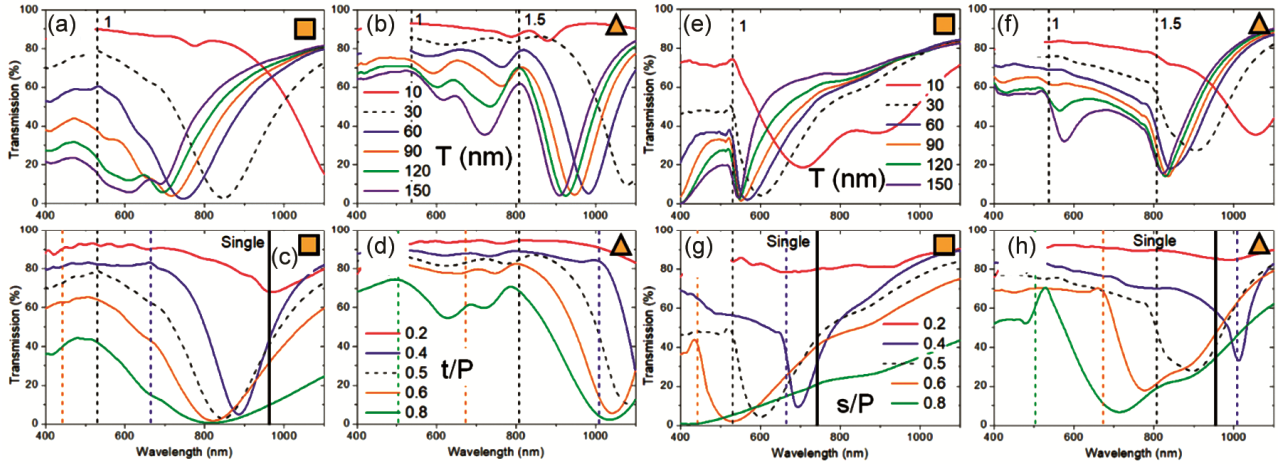

Fig. 6 — Comparison of Au (a-d) and Al (e-h) nanoarray simulated transmission spectra of square (a, c, e, and g) and triangle (b, d, f, and h). (a, b, e, and f) shows the height variation and (c, d, g, and h) shows the respective t/P and s/P ratios. The side of square and triangle were kept as 177.25 nm and 269.35 nm to keep the volume equal to the disc of diameter 200 nm. The nanoarray was at air glass interface for θ = 0°. The vertical dashed lines represent lattice resonance, (1 0) diffraction edge, and the number beside is the refractive index for the lattice resonance. No number pertains to the resonance due to glass environment (n=1.5). Solid line represents the single disc resonance.

thicknesses which are shown in Fig. 6 (e,f). Comparing Au and Al, it can be inferred from Fig. 6 (b,f), the lattice resonance due to air (n=1) was more clearly observed for Al. The lower losses in the UV region, as seen in Fig. 1(c) was the clear contributor to the aforementioned phenomenon. A similar trend was also seen in Fig. 6 (a,e). Furthermore, for similar sizes, the coupling effect was observed more clearly for Al square and triangle in the Fig. 6 (g,h) due to the increased proximity of the single particle resonance to the lattice resonance. The effect of polarization was also checked using refractive index variation plots in Fig. S1, Fig. S2, and Fig. S3 (supplementary material); it was observed that the shift in the resonance wavelengths was not very significant for the respectively comparable cases for $\theta = 45°$ for square nanoarray and $\theta = 60°$ and $90°$ for triangle nanoarray as compared to the $\theta = 0°$ polarization.

3.4 Sensitivity comparison

The effect of the material and the shape of the nanoarray was quantified using a parameter that had numerous practical applications. Nanoarrays are often used as chemical and biosensors, and they work on the principle that a change in the surrounding refractive index is created by the targeted molecule. This change in refractive index leads to shift in the resonance wavelength which can be observed in the transmission spectrum. The refractive index based sensing has already been used for the detection of bacteria[42], viruses[43], biomarkers[44], heavy metals[45], pesticides[46] *etc*. The sensitivity of these sensors is defined as the ratio of change in wavelength to the variation refractive index. Therefore, simulations were performed by varying n_1 from 1 to 2, the volume of the particle in the array being equal to a disc with a diameter of 200 nm and a thickness of 30 nm. To compare the best performing structures, the refractive index variation was performed when the periodicity of the lattice was equal to the single particle resonance of the structure. The single particle resonance of the structures was measured from the Fig. 3, thereby, the sensitivity comparison was performed for the optimal coupling condition as shown in Fig. 7(a-g). It was observed that, when the surrounding of the nanostructures became homogeneous ($n_1 = n_2 = 1.5$), the largest Fano like resonance was observed. As expected, the resonance wavelength was at shorter wavelengths for Al as compared to Au. Comparing the sensitivity, the triangle displayed the highest sensitivity, followed by the square and the disc nanoarray, as shown in Fig. 8. Furthermore, Au showed better sensitivity than Al due to the larger losses in Al. The sensitivity comparison was also performed for the nanostructures with periods

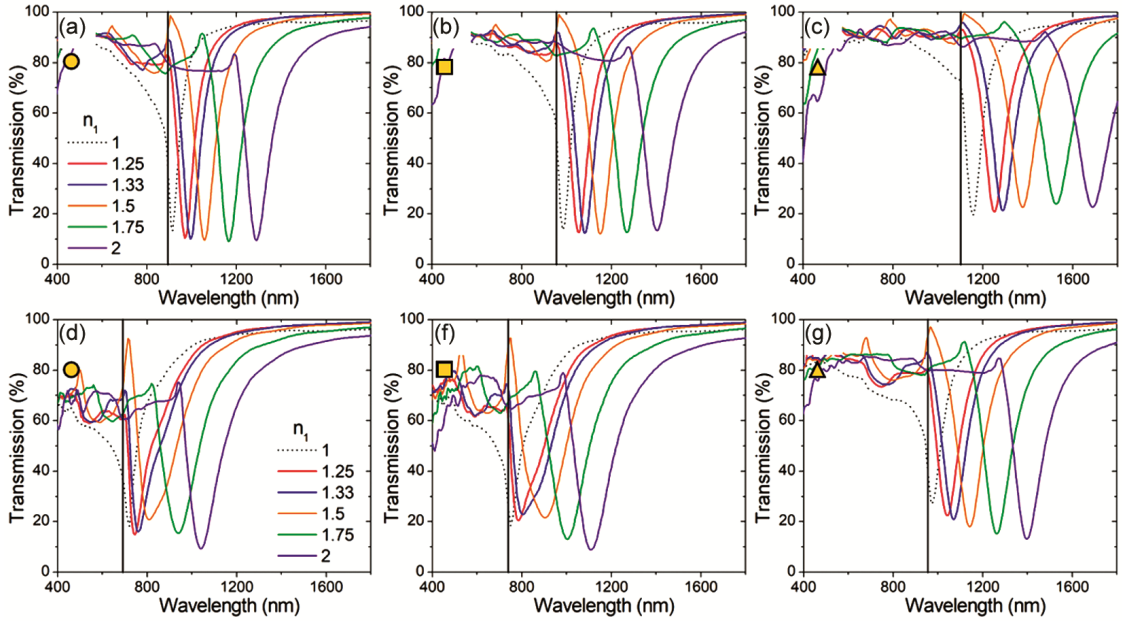

Fig. 7 — Refractive index (n_1) variation in Au (a-c) and Al (a-c) nanoarray for disc (a, e), square, (b, f), and triangle (c, g) shapes. The sloid vertical line represents the single particle resonance. The side of square and triangle were kept as 177.25 nm and 269.35 nm to keep the volume equal to the disc of diameter 200 nm. The square lattice periodicity was equal to the coupling condition of the single particle resonance at air glass interface.

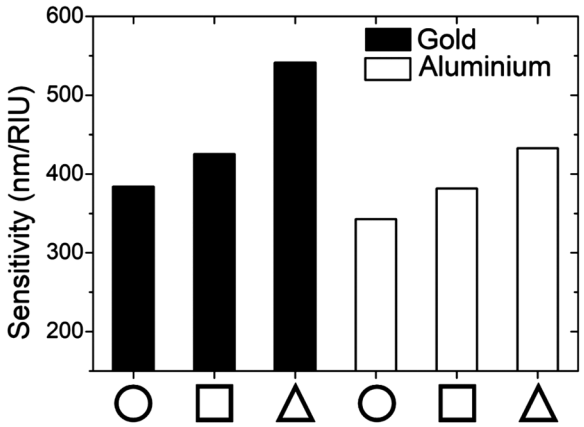

Fig. 8 — Sensitivity comparison of Au and Al nanoarray of disc, square and triangle nanoarrays (at the optimal coupling condition). Volume equal to disk of diameter 200 nm and thickness 30 nm.

Table 1 — Sensitivity comparison of nanopatterns in literature.

Configuration	Sensitivity (nm/RIU)	Reference
Nanograting	73	[47]
Nanodisks array	116	[48]
Plus shaped rod array	250	[49]
Elliptical nanodisk array	327	[50]
Nanocone array	450	[51]
Nanohole array	481	[52]
Nanoellipsoid array	484	[53]
Triangle nanoarray	541	This work
C shaped nanorod array	600	[54]
Sinusoidal nanograting	717	[55]
Nanocrescent array	879	[56]

equivalent to d/P = 0.5 (not at the optimal coupling condition) as shown in Fig. S4. The sensitivity was much lower than for the structures at optimal coupling condition.

Table 1 shows the sensitivity comparison of the various nanopatterns available in literature. The sensitivity of the triangle nanoarray was comparable to the configurations in the literature. Furthermore, from Table 1, it can be inferred that more complicated geometries (crescent shaped array[54], sinusoidal grating[55], and C shaped nanorod array[56]) had higher sensitivities than the conventional shaped arrays. Therefore, this confirms that geometries with more potential for hotspots are highly suitable for sensing applications.

4 Conclusion

The geometric and material parameters of nanoarrays on a glass substrate were studied. The coupling effect of the lattice resonance with the single nanostructure resonance was observed for larger sized structures (disk of diameter 200 nm). The coupling of the aforementioned resonances resulted in stronger resonance in the transmission spectra. The increase in thickness of the structures led to increased confinement of the EM wave and created higher order poles along with the major dipole response. Al nanoarrays displayed resonance at shorter wavelengths than Au; moreover, resonance in the UV region was also observed in nanoarrays of Al. However, in the visible region, the resonances were weaker due to increased material losses. The refractive index variation with resonance wavelength (sensitivity) was studied to study the practical use of these nanoarrays. The overlap of the lattice resonance with the single structure resonance was considered the optimal coupling condition. Sensitivity at the coupling condition was the highest. The best sensitivity was observed for the Au triangle nanoarray (541 nm/RIU), which was high compared to conventionally shaped sensing substrates in literature. Higher sensitivity was observed in literature for unconventional shapes, such as creset shaped nanoarrays and C shaped nanorods. Therefore, confirming that geometries with hotspots at the optimal coupling condition are highly suitable for sensing applications.

Acknowledgments

The authors are grateful to Indian Institute of Technology Ropar and Ministry of Education, Government of India, for providing PhD scholarship. N. Sardana is thankful to Department of Science and Technology (DST), for funding through Scheme for Young Scientists and Technologists (SYST) SP/YO/2021/2098 grant.

References

1 Dolan J A, Wilts B D, Vignolini S, Baumberg J J, Steiner U & Wilkinson T D, *Adv Opt Mater*, 3 (2015) 12.
2 Liu J, Jalali M, Mahshid S & Wachsmann-Hogiu S, *Analyst*, 145 (2020) 364.
3 Kasani S, Curtin K & Wu N, *Nanophotonics*, 8 (2019) 2065.
4 Baranov D A, Dmitriev P A, Mukhin I S, Samusev A K, Belov P A, Simovski C R & Shalin A S, *Appl Phys Lett*, 106 (2015) 171913.
5 Garnett E & Yang P, *Nano Lett*, 10 (2010) 1082.
6 Wei W, Bai F & Fan H, *Angew Chemie Int Edn*, 58 (2019) 11956.
7 Homola J, Surface Plasmon Resonance Based Sensors, In: Springer Ser Chem Sensors Biosens. 1st Edn Springer, Berlin, Heidelberg, (2006).
8 Maier S A, Plasmonics: Fundamentals and Applications, Springer US, (2007).
9 Mayer K M & Hafner J H, *Chem Rev*, 111 (2011) 3828.
10 Pandey P S, Raghuwanshi S K & Kumar S, *IEEE Sens J*, 22 (2022) 1069.

11 Maurer T, Adam P M & Lévêque G, *Nanophotonics*, 4 (2015) 363.
12 Oates T W H, Wormeester H & Arwin H, *Prog Surf Sci*, 86 (2011) 328.
13 Rycenga M, Cobley C M, Zeng J, Li W, Moran C H, Zhang Q, Qin D & Xia Y, *Chem Rev*, 111 (2011) 3669
14 Singh G P & Sardana N, *Bull Mater Sci*, 45 (2022) 241.
15 Yoon B K, Hwang W, Park Y J, Hwang J, Park C & Chang J, *Macromol Res*, 13 (2005) 435.
16 Keil M, Wetzel A E, Wu K, Khomtchenko E, Urbankova J, Boisen A, Rindzevicius T, Bunea A-I & Taboryski R J, *Nanoscale Adv*, 3 (2021) 2236.
17 Liu R, Cao L, Liu D, Wang L, Saeed S & Wang Z, *Nanomaterials*, 13 (2023) 1818.
18 Zhao Z-J, Hwang S, Bok M, Kang H, Jeon S, Park S-H & Jeong J-H, *ACS Appl Mater Interfaces*, 11 (2019) 30401.
19 Heltzel A, Theppakuttai S, Chen S C, Howell J R, *Nanotechnology*, 19 (2008) 025305.
20 Robatjazi H, Bahauddin S M, Macfarlan L H, Fu S & Thomann I, *Chem Mater*, 28 (2016) 4546.
21 Nishijima Y, Rosa L & Juodkazis S, *Opt Express*, 20 (2012) 11466.
22 Hasan R M M & Luo X, Nanolithography: Status and challenges. In: 2017 23rd *Int Conf Autom Comput*, (2017) 1.
23 Potejanasak P, *Crystals*, 11 (2021) 1452.
24 Luo S, Mancini A, Wang F, Liu J, Maier S A & de Mello J C, *ACS Nano*, 16 (2022) 7438.
25 Mudachathi R & Tanaka T, *Sci Rep*, 7 (2017) 1199.
26 Tassin P, Zhang L, Koschny T, Economou E N & Soukoulis C M, *Phys Rev Lett*, 102 (2009) 053901.
27 Zhao X, Huang R, Du X, Zhang Z & Li G, Ultrahigh- Q Metasurface Transparency Band Induced by Collective–Collective Coupling, *Nano Lett*, (2024).
28 Yang Y, Wang W, Boulesbaa A, Kravchenko I I, Briggs D P, Puretzky A, Geohegan D & Valentine J, *Nano Lett*, 15 (2015) 7388.
29 Taubert R, Hentschel M, Kästel J & Giessen H, *Nano Lett*, 12 (2012) 1367.
30 Chen Z, Taflove A & Backman V, Opt Express, 12 (2004) 1214.
31 Xue X, Fan Y, Segal E, Wang W, Yang F, Wang Y, Zhao F, Fu W, Ling Y, Salomon A & Zhang Z, *Mater Today*, 46 (2021) 54.
32 Rakić A D, Djurišić A B, Elazar J M & Majewski M L, *Appl Opt*, 37 (1998) 5271.
33 Mäntynen H, Lipsanen H & Anttu N, *Symmetry (Basel)*, 13 (2021) 752.
34 Lv Z, Liu L, Zhangyang X, Lu F & Tian J, *Appl Phys A*, 126 (2020) 152.
35 Li J, Kan Q, Wang C & Chen H, *Chin Opt Lett*, 9 (2011) 090501.
36 Jensen T, Kelly L, Lazarides A & Schatz G C, *J Clust Sci*, 10 (1999) 295.
37 Palanisamy S, Zhang X & He T, *Sci China Chem*, 59 (2016) 387.
38 Liao P F & Wokaun A, *J Chem Phys*, 76 (1982) 751.
39 Sievers J, Below M, Reinhardt C, Heyroth F, Schlenker S, Schmidt G, Sprafke A & Schilling J, *J Appl Phys*, 130 (2021).
40 Technique O, Technologies J, Clayton K, Khor J, Wereley S T & Lafayette W, Encyclopedia of Nanotechnology. Bhushan B, Edtd, Dordrecht: Springer Netherlands, (2016).
41 Kravets V G, Kabashin A V, Barnes W L & Grigorenko A N, Chem Rev, 118 (2018) 5912.
42 Taylor A D, Ladd J, Yu Q, Chen S, Homola J & Jiang S, *Biosens Bioelectron*, 22 (2006) 752.
43 Islam A, Haider F, Ahmmed Aoni R & Ahmed R, *Opt Express*, 30 (2022) 40277.
44 Nankali M, Einalou Z, Asadnia M & Razmjou A, *ACS Appl Bio Mater*, 4 (2021) 1958.
45 Forzani E S, Zhang H, Chen W & Tao N, Environ Sci Technol, 39 (2005) 1257.
46 Gouzy M-F, Keß M & Krämer PM, *Biosens Bioelectron*, 24 (2009) 1563.
47 Sun P, Zhou C, Jia W, Wang J, Xiang C, Xie Y & Zhao D, *Opt Commun*, 459 (2020) 124946.
48 Khan Y, Li A, Chang L, Li L & Guo L, SensActuators B Chem, 255 (2018) 1298.
49 Cheng D, Cao S, Ding S, Zhan S & Gao Y, *Results Phys*, 17 (2020) 103143.
50 Lee S-W, Lee K-S, Ahn J, Lee J-J, Kim M-G & Shin Y-B, *ACS Nano*, 5 (2011) 897. doi:10.1021/nn102041m
51 Hongyu W & Ni L, *Chem Phys*, 579 (2024) 112167.
52 Im H, Sutherland J N, Maynard J A & Oh S-H, *Anal Chem*, 84 (2012) 1941.
53 Nair R V, S AT & Menon A U, Orientation-Specific Plasmonic Biosensor for Alzheimer's Disease Detection Using Graphene-Wrapped Au Nano ellipsoids, *Plasmonics*, (2023). doi:10.1007/s11468-023-02006-5
54 Päivänranta B, Merbold H, Giannini R, Büchi L, Gorelick S, David C, Löffler J F, Feurer T & Ekinci Y, *ACS Nano*, 5 (2011) 6374.
55 Iqbal T, Noureen S, Afsheen S, Khan M Y & Ijaz M, *Opt Mater (Amst)*, 99 (2020) 109530.
56 Bukasov R, Ali T A, Nordlander P & Shumaker-Parry J S, *ACS Nano*, 4 (2010) 6639.